ELSEVIER

Nuclear Instruments and Methods in Physics Research A 401 (1997) 365–378

NUCLEAR INSTRUMENTS & METHODS IN PHYSICS RESEARCH Section A

Measurements of the response function and the detection efficiency of an NE213 scintillator for neutrons between 20 and 65 MeV

S. Meigo*

Japan Atomic Energy Research Institute, Tokai, Ibaraki-ken 319-11, Japan

Received 23 May 1997

Abstract

For neutrons 25, 30 and 65 MeV, the response functions and detection efficiencies of an NE213 liquid scintillator were measured. Quasi-monoenergetic neutrons produced by the $^{7}Li(p,n_{0,1})$ reaction were employed for the measurement and the absolute flux of incident neutrons was determined within 4% accuracy using a proton recoil telescope. Response functions and detection efficiencies calculated with the Monte Carlo codes, CECIL and SCINFUL, were compared with the measured data. It was found that response functions calculated with SCINFUL agreed better with experimental ones than those with CECIL, however, the deuteron light output used in SCINFUL was too low. The response functions calculated with a revised SCINFUL agreed with the experimental ones quite well even for the deuteron bump and peak due to the $C(n,d_0)$ reaction. It was confirmed that the detection efficiencies calculated with the original and the revised SCINFULs agreed with the experimental data within the experimental error, while those with CECIL were about 20% higher in the energy region above 30 MeV.

PACS: 29.40.Mc; 29.30.Hs; 25.40.Dn; 25.40.Fq

Keywords: NE213; Detection efficiency; Response functions; SCINFUL; C(n,z) reactions; Proton recoil telescope

1. Introduction

Applications of high-energy particle accelerators are rapidly growing in many fields. For examples, Japan Atomic Energy Research Institute (JAERI) [1] and Los Alamos National Laboratory (LANL) [2] have proposed actinide-transmutation systems based on high-energy proton accelerators. Intensive neutron sources based on the spallation reaction are being newly developed at National Laboratory for High Energy Physics of Japan (KEK) [3] and the European institutes (European Spallation Source, ESS) [4]. In such fields, the energy of neutrons produced in targets and structural materials extend up to 100 MeV or higher. For the design of these facilities, therefore, detailed data are required on neutron reaction cross sections and the neutron transport in bulk materials. In the measurements of those quantities by the time-of-flight (TOF) technique, an organic scintillator is widely used [5–9]. In Ref. [8,9], NE213 scintillators (12.7 cm in diameter and 12.7 cm long) were employed to measure

* Corresponding author. Tel.: + 81 29 282 5356; fax: + 81 29 282 5663; e-mail: meigo@linac.tokai.jaeri.go.jp.

PII S0168-9002(97)01061-9

neutron spectra. These measurements require the detection efficiency which is the integral value of the response function over the light output of the scintillator.

The detection efficiency and response functions for neutrons are usually calculated with Monte Carlo codes. The code O5S [10] has been used widely for neutronics studies up to 20 MeV. In 1986, SCINFUL [11] was developed by Dickens to extend the neutron-energy range up to 80 MeV by improving O5S. For wide energy range, above several hundred MeV, the code STANTON [12] was developed by Stanton and the code CECIL [13] by Cecil et al., as its improvement.

These codes reproduce the response functions fairly well for neutrons below 20 MeV. In the energy region above 20 MeV, however, the calculated response functions and efficiencies show discrepancies. For example, the efficiencies calculated by CECIL are systematically higher by 15% than those by O5S [14]. It is necessary to measure the response functions and detection efficiency of scintillators for validating and improving the calculation codes.

In the present work, the response function and neutron detection efficiency of an organic scintillator, NE213, were measured using 25, 30 and 65 MeV quasi-monoenergetic neutrons produced via the ^{7}Li(p,n$_{0,1}$) reaction. The absolute neutron flux was measured by a proton recoil telescope (PRT) with high accuracy. The response functions and detection efficiencies calculated with CECIL and SCINFUL were compared with the experimental results.

2. Experimental procedure

2.1. NE213

An NE213 scintillator (NT Technology Inc.) was used. It was of cylindrical shape of 12.7 cm in diameter and 12.7 cm long. The density and the hydrogen-to-carbon ratio of the scintillator were 0.874 g/cm^3 and 1.213, respectively. It was encapsulated in a 1 mm thick bubble-free aluminum container. The scintillator was optically coupled to an R4144 photomultiplier with an E1458 base (Hamamatsu Photonics) which was designed to expand the dynamic range of output pulses for high-energy neutron measurements. In the measurements, the photomultiplier was supplied with − 1700 V. In order to confirm the linearity of pulse heights of the photomultiplier, it was tested at − 1300 V. The results for − 1300 and − 1700 V were consistent with the calibration using gamma-ray sources.

2.2. Experiment setup

The experiments were carried out at Takasaki Ion Accelerators for Advanced Radiation Application (TIARA) and at the tandem accelerator facility of Japan Atomic Energy Research Institute (JAERI). Schematic views of the experimental arrangements at TIARA and the tandem facilities are shown in Figs. 1 and 2, respectively. In the measurements, quasi-monoenergetic neutrons produced via the ^{7}Li(p,n$_{0,1}$)^{7}Be reaction were employed. The n$_0$ and n$_1$ stands for the neutrons produced from the reaction in which the residual

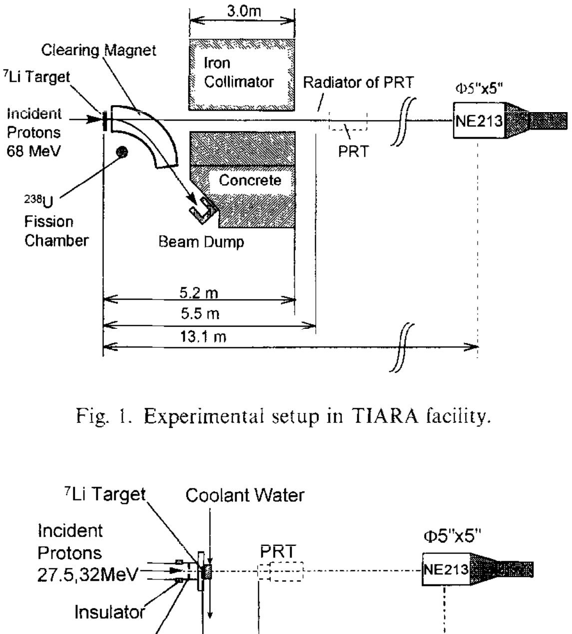

Fig. 1. Experimental setup in TIARA facility.

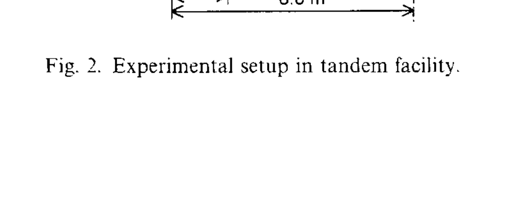

Fig. 2. Experimental setup in tandem facility.

nuclide ^{7}Be is produced ($Q = -1.64$, -2.07 MeV) in the ground and the first excited state, respectively. For the selection of the detection events by monoenergetic neutrons, a time-of-flight technique was employed. The ^{7}Li targets (99%, ^{7}Li) were 5.2 and 1.2 mm thick (2 MeV loss) for the measurements at TIARA and the tandem facilities, respectively.

At TIARA, the measurements were carried out in the Light-Ion Room 3, using incident protons accelerated to 68 MeV by a K-110 AVF cyclotron. The interval between and duration of incident proton pulses were 1.1 μs and 1.5 ns (FWHM), respectively. Protons penetrated the ^{7}Li target and were bent down into a shielded Faraday cup by a clearing magnet. The target was mounted on a water-cooled holder. Neutrons emitted in the 0° direction were guided to the experimental room through a 3 m long iron and concrete collimator. The intensity of the neutron source was monitored by a ^{238}U fission chamber located near the target.

In the tandem facility, the energies of the incident protons were 27.5 and 32 MeV and, therefore, the peak energies of the neutrons were 25 and 30 MeV, respectively. The interval between and duration of the incident proton beam pulses were 250 and 2.0 ns (FWHM), respectively. The target was cooled by water circulated by a pump through an aluminum backing (0.1 mm). The target assembly was electrically isolated and equipped with a secondary electron suppressor by a repeller electrode biased to -300 V. Protons penetrated the target and stopped in water. In the tandem facility, the neutron intensity was monitored by the integrated charge of the incident protons.

2.3. Electronics

In Fig. 3, the circuit diagram for the NE213 detector is shown. A pulse-shape discrimination module of 2160A (Fast Comtec) was employed to eliminate gamma-ray counting. The pulse-height spectra were calibrated using gamma rays from ^{137}Cs, ^{60}Co and ^{241}Am–Be. The energies and the light output for the Compton-edges of these gamma rays are shown in Table 1. The unit of MeVee stands for the light output equivalent to 1 MeV electron. The light output was deduced from the semi-empirical formula of Dietze and Klein [15]. The data for pulse height, pulse shape and flight time were recorded event by event on a hard disk.

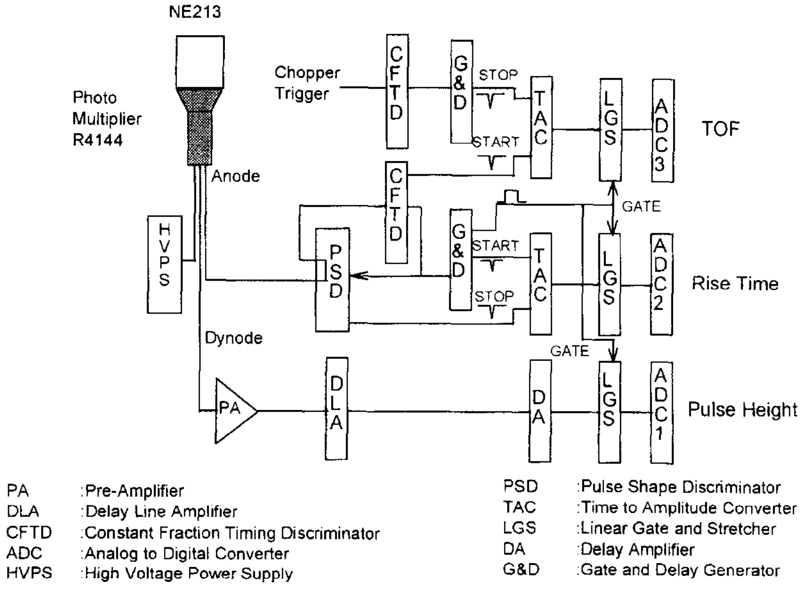

Fig. 3. Block diagram of the NE213 circuit used in the present experiment.

2.4. Proton recoil telescope (PRT)

The intensity of the peak neutrons produced by the $^7Li(p,n_{0,1})$ reaction was measured by proton recoil telescopes (PRTs) [16] which were the most reliable for neutron-flux measurement. PRT consists of a thin polyethylene foil, called radiator, and a telescope for charged-particle detection. PRT observes recoil protons produced through the neutron interaction with the radiator. The neutron detection efficiency of the PRT could be determined precisely from the well-known differential cross section of the H(n,p) reaction in the radiator and the solid angle subtended by the charged-particle detector at the radiator.

Table 1
Light output of a NE213 detector for the half-height of the Compton edge

Gamma ray source	Energy (MeV)	Light output (MeVee)[a]
^{137}Cs	0.662	0.493
^{60}Co	1.173, 1.333	1.074[b]
Am–Be	4.439	4.331

[a] 1 MeVee corresponds to the light output given by 1 MeV electron.

[b] Only one Compton edge is observed, because NE213 has too poor resolution to distinguish two Compton edges. This light output is calculated with the average energy of two gamma rays.

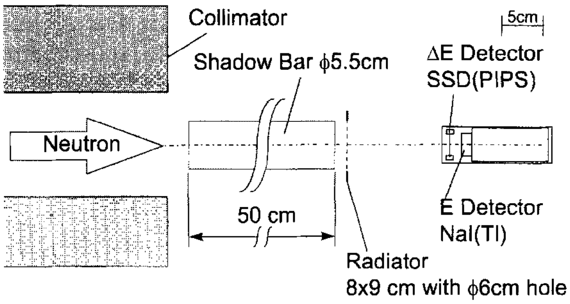

Fig. 4. Schematic view of the PRT used in TIARA facility.

Two types of PRT, as shown in Figs. 4 and 5, were employed in TIARA and tandem facilities, respectively. Protons from a radiator were detected by a ΔE–E telescope that consisted of a ΔE-detector of 900 mm^2 PIPS (Canberra) and an E-detector. NaI(Tl) and BaF_2 scintillators were used as E-detectors in TIARA and tandem facility, respectively. In TIARA facility, the PRT was shielded from the neutron beam by a 50 cm long brass shadow bar to suppress background [16]. The radiator was a polyethylene plate, 0.12–1.0 mm thick and 8×9 cm wide, with a 6 cm diameter hole at the center. It was placed in the air and supported by thin nylon strings. In the tandem facility, a circular polyethylene foil, 0.5 mm thick and 47 mm in diameter, was employed as the radiator.

In order to subtract protons produced in structural materials of PRT, background measurements were performed without the radiator. The background in tandem facility is lower than 5% of the foreground, therefore the shadow bar was not employed. In addition, measurements using a carbon

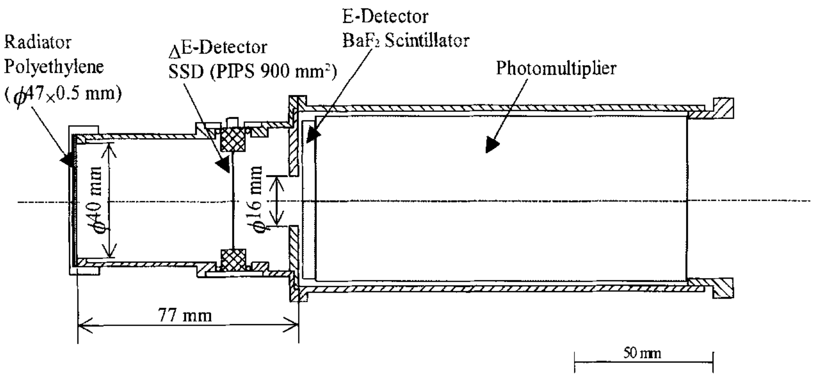

Fig. 5. Schematic view of the PRT used in tandem facility.

foil instead of a radiator were carried out to eliminate the events by the C(n,xp) reaction. The background due to the C(n,xp) reaction was about 5% at 65 MeV, and negligibly small for the lower incident energies.

3. Data reduction

The experimental data were analyzed by the following procedure to deduce response function and detection efficiency of the NE213 scintillator.

3.1. Selection of neutron events

First, the pulse shape was analyzed using the two-dimensional contour plot for the rise time and pulse height. A typical contour plot is shown in Fig. 6. Pulses having long fluorescence tail appear in higher rise-time channels, and thereby, neutron events appear in higher channels than photons. The events for the neutron detection were obtained by using the neutron region shown in Fig. 6. In the neutron region, three ridges are observed corresponding to p, d and α particles produced in the scintillator.

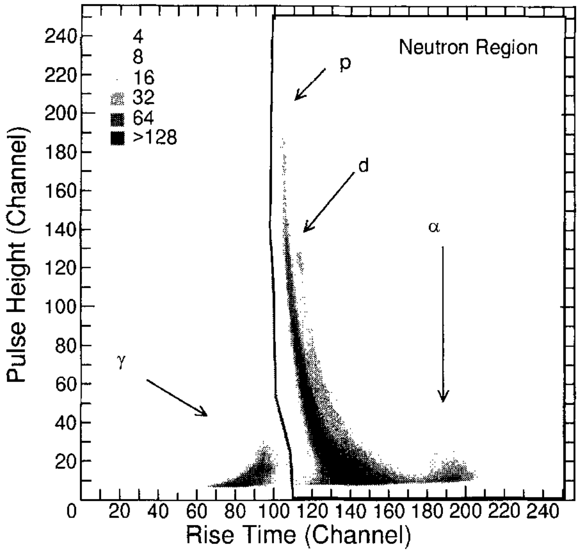

Fig. 6. Scatter plot of the spectrum rise time versus pulse height. Events in the neutron region were taken to eliminate gamma rays.

3.2. Time-of-flight spectrum

After the selection of neutron events, the flight time of the neutrons were analyzed. The TOF spectrum in TIARA is shown in Fig. 7. The spectrum consists of peak due to the ^{7}Li(p,n$_{0,1}$) reaction and a continuous component due to breakup reactions. The energy and the width of the peak are summarized in Table 2. Since the target is thicker than the thickness corresponding to level spacing, the peak includes both n_0 and n_1 neutrons. The detection efficiency and response function of the NE213 detector were derived from the sum counts of the peak area hatched in Fig. 7.

3.3. Flux of peak neutrons

The flux of the peak neutrons was obtained from the counts of the PRT. The energy spectra of recoil protons were deduced from ΔE–E spectra free from the gamma and the deuteron contributions. The energy scale was calibrated by the light-output response of a NaI(Tl) or a BaF_2 scintillator, and the peak energy was determined by the TOF measurement. The neutron flux at PRT is given by

$$\phi(E_n) = \frac{1}{L^2\varepsilon(E_n)}\frac{dE_p}{dE_n}Y(E_p), \tag{1}$$

where L is the distance between the target and the center of radiator, ε the detection efficiency of PRT, E_p the observed proton energy, E_n the incident neutron energy and Y the yield of recoil protons. The detection efficiency ε is obtained using the following equation:

$$\varepsilon(E_n) = N\tau D\int dS_r\int dS_d\frac{1}{l^2d^3}\frac{d\sigma}{d\Omega}(E_n), \tag{2}$$

where N is the number density of hydrogen in the radiator, τ the thickness of the radiator, D the distance between centres of the radiator and the detector, dS_r and dS_d differential surface areas of the radiator and the detector, respectively, l the distance between the target and the n–p collision point, d the distance between the n–p collision

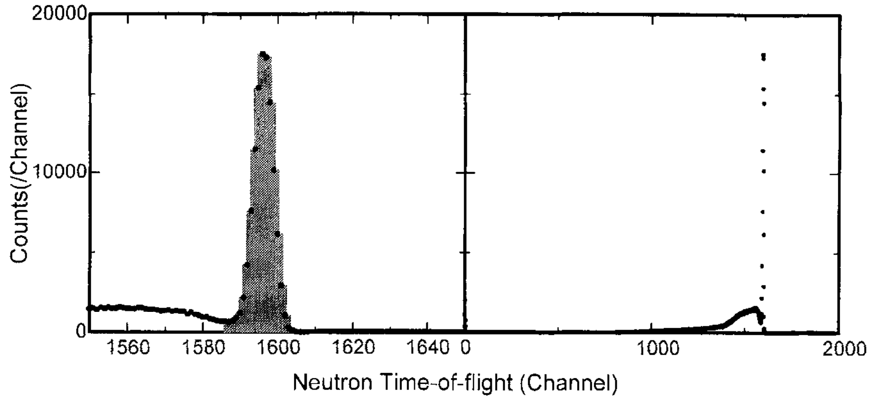

Fig. 7. Time-of-Flight spectrum for the $^{7}Li(p,xn)$ neutrons in TIARA by NE213 detector (left: peak region, right: the whole region). The hatched area is used to obtain the response function and detection efficiency of the NE213.

Table 2
Detection efficiency and error obtained in the present experiment

Incident energy of proton (MeV)			27.5	32	68
Peak energy of neutron (MeV)			25	30	65
FWHM (MeV)			2.2	2.2	2.4
Detection efficiency (%)		^{60}Co Bias	23.7	22.9	14.7
		Am–Be Bias	13.2	13.8	11.9
Error		Monitor	1.5	1.5	4.5
	Neutron flux obtained by PRT	Statistical	1.5	1.5	1.7
		Solid angle	1.0	1.0	0.6
		Number density	0.5	0.5	0.5
		ADX for H(n,p)	1.2	1.5	2.6
		Inelastic[a]	0.2	0.3	0.9
		Peak yield[b]	1.0	1.0	0.2
		Subtotal	2.5	2.6	3.3
	Counts of NE213	Statistical	0.3	0.2	0.2
		Solid angle	0.5	0.5	0.5
		PSD[c]	1.5	1.5	1.5
		Subtotal	1.6	1.6	1.6
		Systematic	2.0	2.0	2.0
		Total	4.0	4.1	6.3

[a] Uncertainty for the inelastic scattering of recoil protons.
[b] Peak-yield uncertainty.
[c] Error of the pulse-shape discrimination.

reaction point on the radiator and the recoil proton injection point on the detector, and $d\sigma/d\Omega$ the angular differential cross section of n–p scattering by Shen and Zhang [17]. The proton spectrum was corrected for background, energy loss, efficiency and for the inelastic scattering in the detectors [18]. The neutron spectrum obtained by PRT is described in Section 5.3 in comparison with that by the NE213 detector.

3.4. Neutron detection efficiency

The detection efficiency of the NE213 detector for the peak neutrons was determined from the counts of NE213 divided by the neutron flux obtained by PRT. Corrections were made for dead-time losses and neutron absorption in the air between the NE213 detector and PRT. The detection efficiencies by the present experiment are summarized in Table 2, together with the errors for ^{60}Co and Am–Be biases. In the error estimation, the statistical and systematic errors of the monitor counts, the neutron flux by PRT and the NE213 counts were taken into account. The overall error was 4–6%. It should be noted that the overall error is much smaller than the error analyzed from the $^{7}Li(p,n_{0,1})$ cross section and the target thickness.

4. Comparison between experiment and calculation

Using the experimental data, the calculations with CECIL and SCINFUL are examined. The causes of deviations of calculation results from the experimental ones are traced and eliminated to improve the codes. The differential n–p scattering and C(n,z) cross sections used in the codes are compared with experimental and evaluated ones.

4.1. CECIL and SCINFUL codes

CECIL takes account of seven reaction channels. i.e. H(n,p), C(n,n), C(n,$x\gamma$), C(n,np), C(n,α), C(n,n'3α) and C(n,2n). In the original version of CECIL, the gamma rays produced from C(n,$x\gamma$) reactions are taken into account in the response functions and detection efficiencies, while they are rejected in the experiment. In order to compare with the experiment, the contribution of the C(n,$x\gamma$) reaction was excluded in the calculations.

The code of SCINFUL deals with 39 reaction channels finally, starting from 11 initial reactions, i.e. H(n,p), C(n,n), C(n,n'), C(n,2n), C(n,p), C(n,np), C(n,d), C(n,^{3}He), C(n,α), C(n,n'3α), C(n,$x\gamma$). The calculation of the C(n,$x\gamma$) reaction was omitted. SCINFUL takes account of the light attenuation in the scintillator. The light attenuation coefficient was determined as 8×10^{-3} cm^{-1}, to reproduce the proton edges of the experimental response functions for neutrons below 20 MeV.

In calculations with both codes, 1×10^5 initial collision histories were accumulated.

4.2. Comparisons of response functions

The experimental response functions are shown in Fig. 8, together with CECIL and SCINFUL results for the same neutron energies and peak widths. In this figure, the abscissa and vertical axis represent, respectively, the electron equivalent light output (MeVee) and the number of counts per incident neutron and MeVee. In the response functions for 25, 30 and 65 MeV neutrons, recoil proton edges are observed to be 17, 20 and 48 MeVee, respectively, as expected. In the responses for 30 and 65 MeV, bump and peak are apparent around 7 and 32 MeVee, respectively. These are due to deuterons produced by the pick-up reaction of C(n,d_0) (Q = − 13.73 MeV) and are found at the higher light-output channel in the deuteron ridge shown in Fig. 6.

The calculation with CECIL agreed with the experimental data for 25 and 30 MeV neutrons, except at the recoil proton edges and below 1.5 MeVee. The larger values at proton edges occur because CECIL does not take account of the light

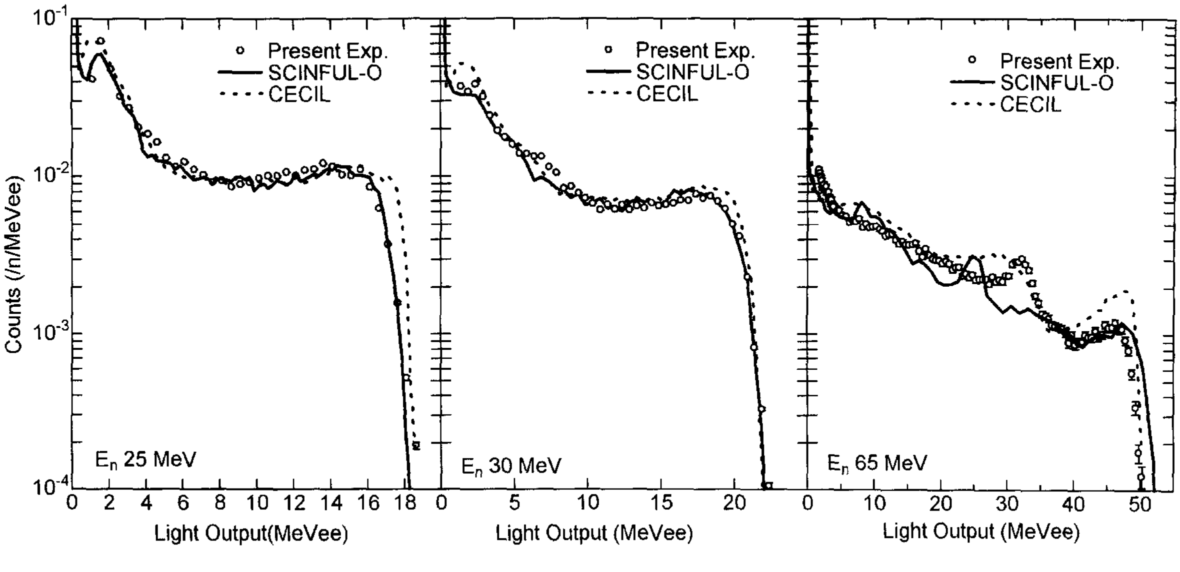

Fig. 8. Response functions of the NE213 detector by the present experiment in comparison with those calculated with CECIL and SCINFUL.

attenuation. For 65 MeV neutrons, however, CECIL overestimates the experiment at the recoil edge and in the light-output region above 5 MeVee (cf. Sections 4.4 and 4.5). Besides, CECIL does not reproduce the deuteron peak, because it does not take the C(n,xd) reaction channel into account.

SCINFUL shows better agreement with the experimental data than CECIL for the three neutron energies. However, the calculated light output of deuteron peak for 65 MeV is markedly lower than the experimental data. This is attributed to the inadequate light output data for deuteron. Improvement of this is described in Section 5.1. On the contrary, the light output for proton edge in 65 MeV data is higher than the experiment. This will not introduce serious error for the detection efficiency for bias lower than ~20 MeVee because the light output of the recoil edge is very well reproduced for neutrons up to 30 MeV. In addition, around 8 MeVee, SCINFUL gives a peak that is not existing in the experimental result. Concerning the above discrepancies, the cross-section data used in the code were examined, in particular, for n–p scattering and the C(n,z) reactions.

4.3. Comparison of detection efficiencies

By integrating the response functions over the light output, detection efficiencies were obtained. These are compared with the experimental data for ^{60}Co and Am–Be biases in Fig. 9. In this figure, the experimental data for lower-energy neutrons by Verbinski et al. [19] are also shown. The results calculated with the original SCINFUL (SCINFUL-O) reproduce the experimental data within experimental errors. The efficiencies calculated with CECIL agree well with the experimental data for neutrons below ~15 MeV, but for the neutrons above ~20 MeV, are higher than the experiment and SCINFUL by about 20%.

In order to trace the origin of this overestimation of CECIL, the contribution of n–p and C(n,z) cross sections for the detection efficiency was examined by removing hydrogen or carbon atoms from the scintillator. The results for ^{60}Co bias are shown in ig. 10. From the comparison, it is proved that the C(n,z) contribution is significant above 30 MeV and the overestimation of CECIL is due to a large

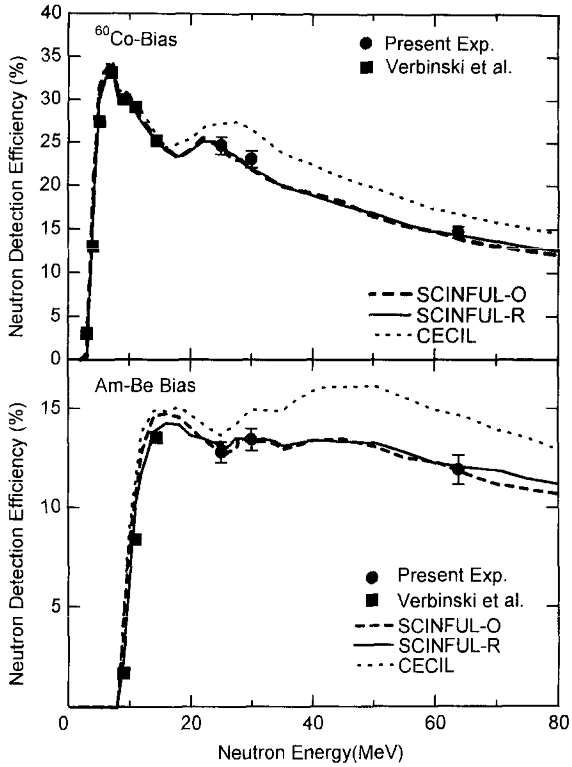

Fig. 9. Detection efficiency of the NE213 detector for ^{60}Co and Am–Be biases.

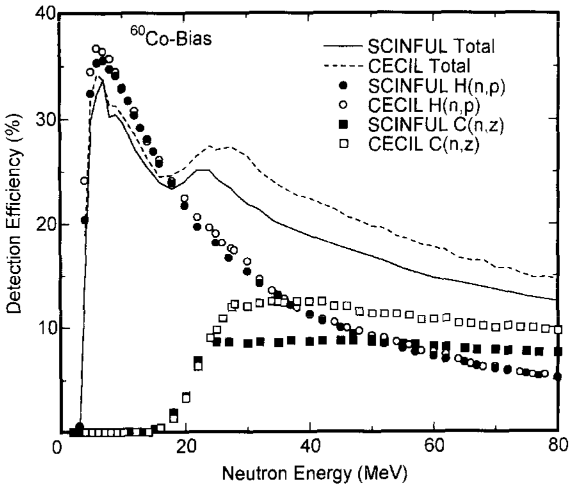

Fig. 10. Contribution of H(n,p) and C(n,z) reactions to the detection efficiency for ^{60}Co bias.

C(n,z) contribution. This overestimation is also found in the result for Am–Be bias.

In the energy region below 15 MeV, the contribution of the n–p scattering is larger than the total contribution. It is caused by the fact that the escape of neutrons from the scintillator due to the C(n,n) reaction is a significant process in the calculation of the total contribution.

4.4. H(n,p) reaction cross section data in the code

The total and differential n–p scattering cross sections used in CECIL and SCINFUL are compared with the results of phase-shift analysis by Arndt [20]. The numerical data of phase-shift analysis are derived from Ref. [21], which gives the differential cross section as the Legendre expansion coefficient. The total cross section used in CECIL agreed with the phase-shift analysis data within 3%, except an overestimation by around 5% in the energy region between 50 and 60 MeV.

SCINFUL calculates the total n–p cross section using the formula of Gammel [22]. The calculated values agreed with the phase-shift analysis data within 2% below $\sim$50 MeV, but above $\sim$50 MeV become lower with increasing neutron energy.

In Fig. 11, the angular differential cross sections (ADXs) used in CECIL and SCINFUL are compared with the experimental data [23–25] and the phase-shift analysis data. In CECIL, the ADX ($\mathrm{d}\sigma/\mathrm{d}\Omega$) is isotropic below 29.9 MeV, and is presented by the following formula above 30 MeV:

$$\frac{\mathrm{d}\sigma}{\mathrm{d}\Omega} \propto 90/(E+90) + 3E/(E+90)\mu^2. \tag{3}$$

where E is the neutron energy in the laboratory system (MeV) and μ the direction cosine for recoil proton in the center-of-mass system. Fig. 11 shows that the ADXs in CECIL are too large at both forward and backward angles above 30 MeV. The overestimation in the forward angles gives large sensitivity at the recoil edge in the response functions calculated with CECIL as observed in Fig. 8.

The ADXs used in SCINFUL, on the contrary, agree better with the experimental ones, and thereby, the recoil edges calculated with SCINFUL are closer to the experiment. Nevertheless, in comparison with the phase-shift analysis data, both the total and angular differential cross sections differ

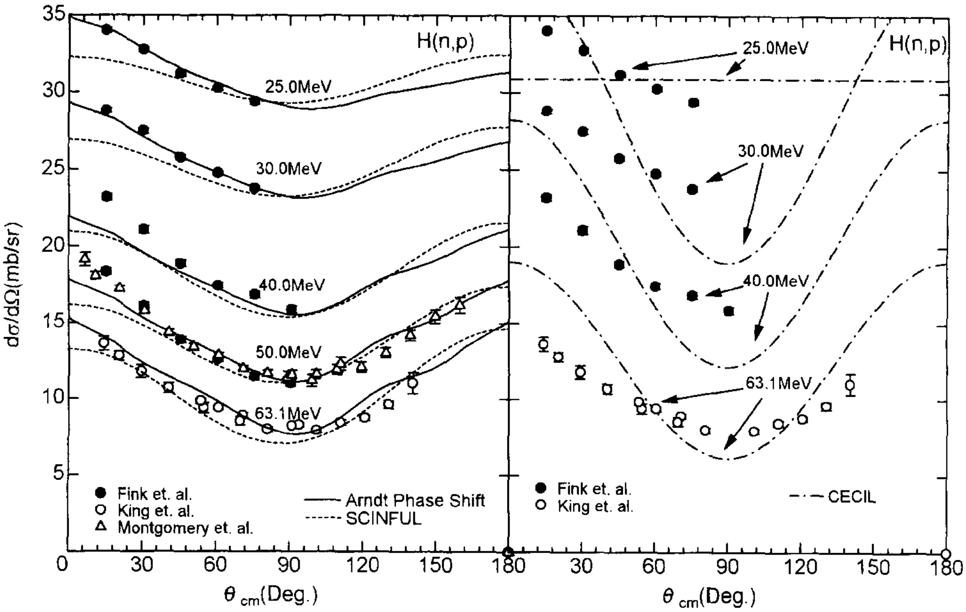

Fig. 11. The angular differential cross sections for n–p scattering in CECIL and SCINFUL compared with th experimental data in Ref. [23–25] and the phase-shift analysis given by Arndt [20, 21]. The cross sections are shown in the center-of-mass system.

appreciably. Therefore, SCINFUL was revised by changing n–p cross sections as described in Section 5.1.

In the analysis of neutron-flux measurement by PRT, the ADXs given by Shen and Zhang [17] were employed. For the peak energy of the incident neutrons, these ADXs agreed with those by Arndt within 3%.

4.5. Energy differential cross sections for C(n,xp), C(n,xd) and C(n, xα) reactions

The energy differential cross sections (EDXs) for C(n,z) in the codes are compared with the experimental data [26,27] and with those evaluated at Lawrence Livermore National Laboratory (LLNL) [28] for 27.4 and 60.7 MeV neutrons in Fig. 12. The EDXs were extracted from CECIL and SCINFUL codes. Sums of the EDXs for C(n,xp) and C(n,xd) are also shown, because CECIL does not deal with the C(n,d) reaction separately. The sum of EDXs for C(n,xp) and C(n,xd) reactions in CECIL reasonably agrees with the experimental data, except for the high outgoing energy. The EDXs for C(n,xα) reaction in CECIL are, however, remarkably much larger than the experimental data for the high-energy alpha particles. This fact interprets the overestimation of the responses in Fig. 8.

In the case of SCINFUL, on the other hand, the sum of EDXs for C(n,xp) and C(n,xd) reactions

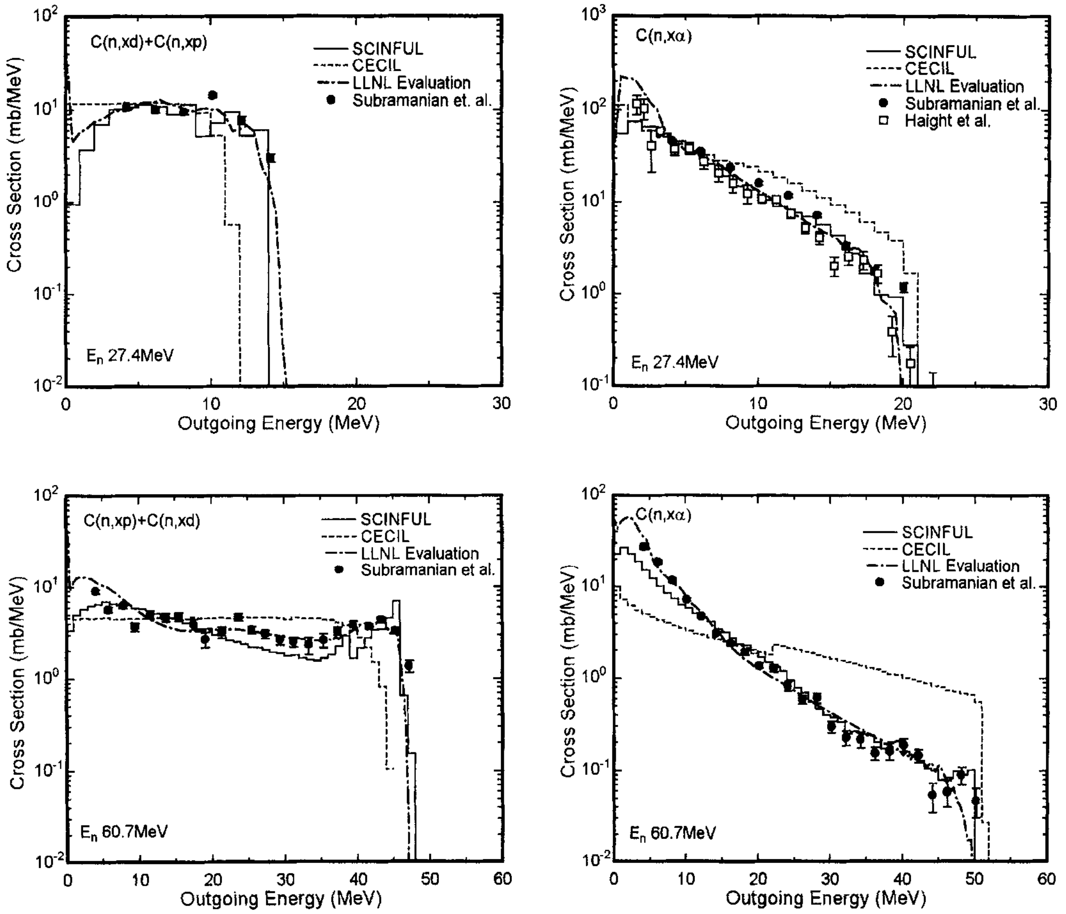

Fig. 12. Changed-particles emission spectrum for the C(n,z) reaction for 27.4 and 60.7 MeV neutrons in CECIL and SCINFUL. Circles and squares stand for experimental data [26,27].

agree with the experimental and LLNL evaluation data better than the case of CECIL. The EDXs for C(n,xα) reaction in SCINFUL are in much better agreement with the experimental data in particular for 60.7 MeV neutrons. The underestimation below ~ 8 MeV of the spectrum will not introduce serious error in the detection efficiency for higher bias than ^{60}Co bias, because the light output for 8 MeV alpha particles is smaller than 1 MeVee.

5. Revision of SCINFUL code

5.1. SCINFUL-R

This section describes the improvement of SCINFUL to eliminate problems described in Section 4. The code was revised by changing the light output for deuterons, and the total and differential n–p scattering cross sections. As described in Section 4.2, the light output of deuteron in SCINFUL was lower than the experiment. Hence, it was replaced with new data modified from the proton light output in SCINFUL on the basis of the empirical formula of Murray and Meyer [29], which characterized the light output by the stopping power for hydrogen isotopes. Fig. 13 shows the relation between the differential light output and stopping power [18] and shows that the differential light output for deuterons is much smaller than that for protons. The deuteron light output was, therefore, rebuilt from the integration of the differential light output for protons given by the least-squares polynomial fit. By this modification, the present light output for deuterons is larger by about 25% than that in the original SCINFUL.

In addition, the total and angular differential cross section data for n–p scattering were replaced with the values by phase-shift analysis [20,21]. Hereafter, the original SCINFUL and the revised one are referred to as SCINFUL-O and SCINFUL-R, respectively.

5.2. Results calculated with SCINFUL-R

The calculated response functions by SCINFUL-R are compared with the experimental ones in Fig. 14. The response functions with SCINFUL-O

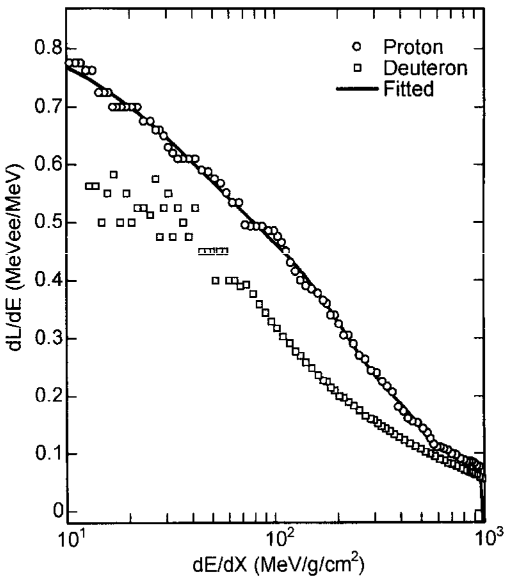

Fig. 13. Relationship between the stopping power and the differential light output used in SCINFUL. The line shows the results of the least-squares fit.

are also shown. The deuteron bump and peak in the response function with the SCINFUL-R agreed with the experimental data quite well. There still remains, however, an artificial bump around 10 MeVee for 65 MeV neutrons. The reason of the bump is not clear. Further investigations will be necessary to understand this bump, while it does not affect the detection efficiency for the ^{60}Co and Am–Be biases as described in below and Section 5.3.

The detection efficiencies calculated with SCINFUL-R are shown in Fig. 9. The results of SCINFUL-R as well as those of SCINFUL-O agree with the experimental ones. In the energy region below 20 MeV, SCINFUL-R for Am–Be bias reproduces the experiment better than SCINFUL-O.

5.3. Detection efficiency calculated with SCINFUL-R for 30–65 MeV neutrons

In the present work, the detection efficiency was not measured for neutrons between 30 and 65 MeV. In order to examine the calculated detection efficiency in this region, the neutron spectra

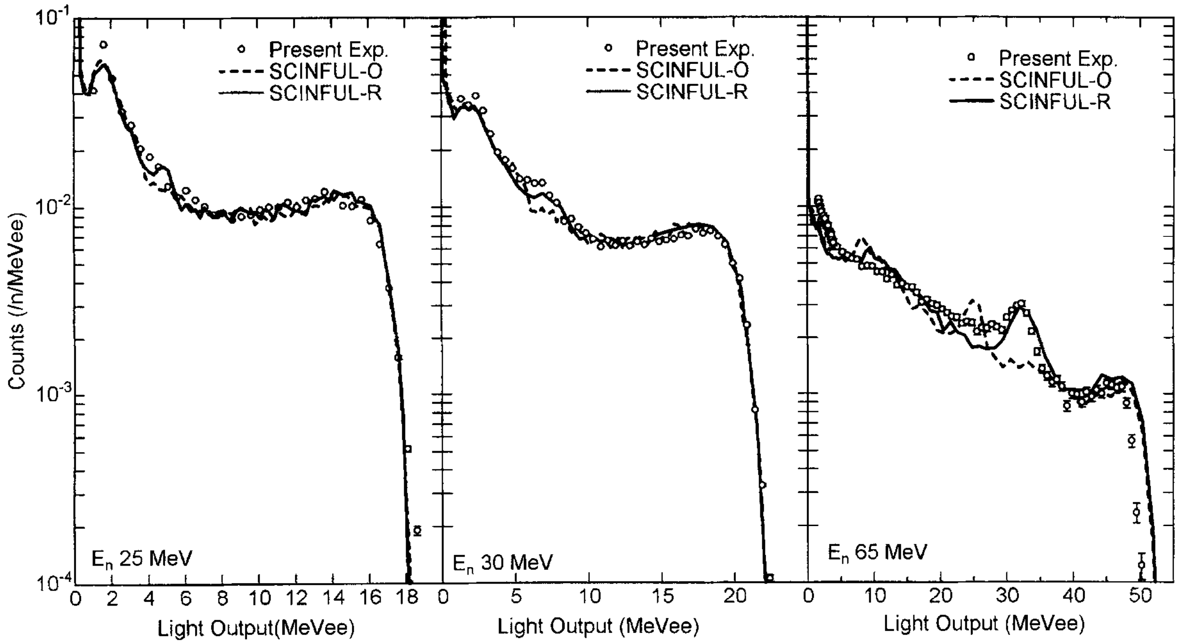

Fig. 14. Response functions by the revised SCINFUL-R.

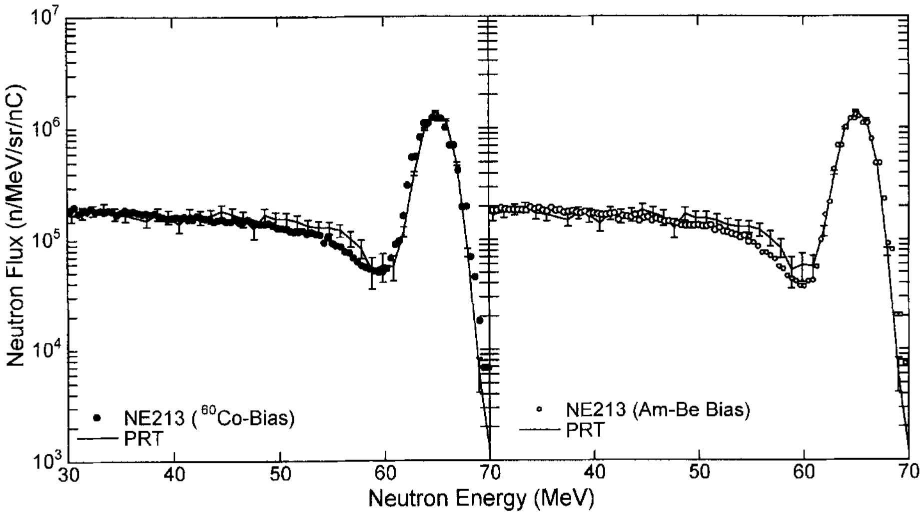

Fig. 15. Comparison of the neutron spectra by the SCINFUL-R and by the PRT measurement.

obtained by the NE213 measurements were compared with those by PRT as shown in Fig. 15 for ^{60}Co and Am–Be bias data. In the peak region, the spectra by NE213 were smeared by the energy resolution of PRT to fit to the PRT data. In the energy region between 30 and 70 MeV, the spectra obtained by the NE213 measurements agree with those by PRT within the experimental error, except the region between 55 and 60 MeV. The disagreement would be attributed to the poor energy resolution of PRT. The NE213 efficiency calculated with SCINFUL-R will be good enough even for the energy region between 30 and 55 MeV.

6. Conclusion

The response function and detection efficiency of an NE213 detector of 12.7 cm diameter and 12.7 cm thickness were measured for neutrons of 25, 30 and 65 MeV. In the measurements, and quasimono-energetic neutrons produced via the $^{7}Li(p,n_{0,1})$ reaction were used and the absolute neutron flux was measured with accuracy better than 4% by a proton recoil telescope (PRT). The overall error of detection efficiency measured in this work was 4–6%.

The experimental results were compared with those calculated with CECIL and SCINFUL. It was found that CECIL overestimates the response function at the proton edge, because of the overemphasis of the angular differential cross section of n–p reaction at forward angle. The response functions calculated with SCINFUL agreed better with experimental ones than those with CECIL. The light output data of deuteron in SCINFUL were revised by the semi-empirical rule of Murray and Meyer, because SCINFUL underestimates the light output for the deuteron peak due to the $C(n,d_0)$ reaction. In addition, the n–p scattering cross sections were replaced with the phase-shift analysis data of Arndt. For the whole incident energies, the responses calculated with the revised SCINFUL (SCINFUL-R) agreed with the experimental data.

The neutron detection efficiency calculated with both SCINFUL-R and -O agreed with the experimental ones within the error of the measurement. The calculated efficiency with CECIL is about 20% higher than the experimental results because of overestimation of $C(n,x\alpha)$ spectra. In the energy region between 3 and 65 MeV, the calculated results with SCINFUL-R are in good agreement with those of the experiment. These facts will suggest that the detection efficiencies set at ^{60}Co and Am–Be bias can be predicted with SCINFUL-R with accuracy better than 4–6%, while slight differences remain for the response function between SCINFUL-R and the experiment.

Acknowledgements

The author would like to thank Drs. H. Nakashima, Su. Tanaka, Sh. Tanaka, M. Yoshioka, T. Kiyosumi, Y. Nauchi, Y. Uno, T. Fukahori, and operation staffs of TIARA and tandem accelerators for their assistance in the experiment. He appreciates Drs. S. Chiba, T. Nakamoto, M. Harada, H. Yasuda, Profs. K. Ishibashi, Y. Watanabe, M. Baba for many useful discussions, and Dr. M. Chadwick for providing the evaluated data file for carbon.

References

[1] T. Takizuka, T. Nishida, H. Takada, S. Meigo, M. Mizumoto, Proc. OECD/NEA Mtg., Argonne National Laboratory, 1993, p. 398.
[2] C.D. Bowman et al., Nucl. Instr. and Meth. A 320 (1992) 336.
[3] N. Watanabe, Proc. 11th Meeting Int. Collaboration Advanced Neutron Sources, (ICANS-XI), KEK, Tsukuba, 1990, p. 471.
[4] K. Gardner, H. Lengeler, G.H. Rees, ESS Report, Ess 95-30M, 1995.
[5] F. Borne et al., Nucl. Instr. and Meth. A 385 (1997) 339.
[6] M.M. Meier, C.A. Coulding, G.L. Morgan, J.L. Ullmann, Nucl. Sci. Eng. 104 (1990) 339.
[7] W.B. Amian, R.C. Byrd, D.A. Clark, C.A. Goulding, M.M. Meier, G.L. Morgan, C.E. Moss, Nucl. Sci. Eng. 115 (1993) 1.
[8] T. Nakamoto, K. Ishibashi, N. Matsufuji, N. Shigyo, K. Maehata, S. Meigo, H. Takada, S. Chiba, M. Numajiri, T. Nakamura, Y. Watanabe, J. Nucl. Sci. Technol. 32 (1995) 828.
[9] S. Meigo, H. Takada, S. Chiba, T. Nakamoto, K. Ishibashi, N. Matsufuji, K. Maehata, N. Shigyo, Y. Wakuta, Y. Watanabe, M. Numajiri, Proc. 13th Meeting of Int. Collaboration on Advanced Neutron Source (ICANS-XIII), Paul Sherrer Institute, PSI Proc.95-02, 1995, p. 442.
[10] R.E. Textor, V.V. Verbinski, ORNL-4160, Oak Ridge National Laboratory, 1968.
[11] J.K. Dickens, ORNL-6436, Oak Ridge National Laboratory, 1988.
[12] N.R. Stanton, COO-1545-92, Ohi State University, 1971.
[13] R.A. Cecil, B.D. Anderson, R. Madey, Nucl. Instr. and Meth. 161 (1979) 439.

[14] H.P. Isaak, P. Heusi, H.S. Pruys, R. Engfer, E.A. Hermes, T. Kozlowski, U. Sennhauser, H.K. Walter, Helv. Phys. Acta 55 (1982) 477.

[15] G. Dietze, H. Klein, Nucl. Instr. and Meth. 193 (1982) 529.

[16] M. Baba, T. Kiyosumi, T. Iwasaki, M. Yoshioka, S. Matsuyam, N. Hirakawa, T. Nakamura, Su. Tanaka, R. Tanaka, Sh. Tanaka, H. Nakashima, S. Meigo, Proc. Int. Conf. on Nuclear Data for Science and Technology, Gatlinburg, 1994, 90.

[17] Q. Shen, J. Zhang, Nucl. Sci. Eng. 117 (1994) 88.

[18] J.F. Janny, Atom. Data Nucl. Data Tables 27 (1982) 147.

[19] V.V. Verbinski, J.C. Courtney, W.R. Burrus, T.A. Love, ORNL-P-993, Oak Ridge National Laboratory, 1965.

[20] R.A. Arndt, Phys. Rev. D 28 (1983) 28.

[21] S. Chiba, S. Morioka, T. Fukahori, J. Nucl. Sci. Technol. 33 (1996) 654.

[22] J.L. Gammel, Fast Neutron Physics, Part 2, Interscience, New York, 1960, ch. 6, p. 2185.

[23] N.S.P. King, J.D. Reber, J.L. Romero, D.H. Fitzgerald, J.L. Ullmann, T.S. Subramanian, F.P. Brady, Phys. Rev. C 21 (1980) 1185.

[24] G. Fink, P. Doll, T.D. Ford, R. Garrett, W. Heeringa, K. Hofmann, H.O. Klages, H. Krupp, Nucl. Phys. A 518 (1990) 561.

[25] T.C. Montgomery, F.P. Brady, B.E. Bonner, W.B. Broste, M.W. McNaughton, Phys. Rev. C 16 (1977) 499.

[26] T.S. Subramanian, J.L. Romero, F.P. Brady, J.W. Watson, D.H. Fitzgerald, R. Garrett, G.A. Needham, J.L. Ullmann, C.I. Zanelli, D.J. Brenner, R.E. Prael, Phys. Rev. C 28 (1983) 521 and Ref. [28].

[27] R.C. Haight, T.M. Lee, S.M. Sterbenz, F.B. Bateman, S.M. Grimes, R. Pedroni, V. Mishra, N. Boukharouba, F.C. Goeckner, C.E. Brient, O.A. Wasson, H. Vonach, Proc. Int. Conf. on Nuclear Data for Science and Technology, Gatlinburg, 1994, p. 311 and Ref. [28].

[28] M.B. Chadwick, L.J. Cox, P.G. Young, A.S. Meigooni, Nucl. Sci. Eng. 123 (1996) 17.

[29] R.B. Muray, A. Meyer, Phys. Rev. 122 (1961) 815.